RECENT DEVELOPMENTS IN THE APPLICATION OF THE INTERDEPENDENCE MODEL OF GRAIN FORMATION AND REFINEMENT

D.H. StJohn[1], X. Hu[2], M. Sun[3], L. Peng[2], H. Dieringa[4]

[1]Centre for Advanced Materials Processing and Manufacturing (AMPAM), School of Mechanical and Mining Engineering, The University of Queensland, St Lucia, Queensland, Australia
[2]Shanghai Jiaotong University, Shanghai, China
[3]University of Shanghai for Science and Technology, Shanghai, China
[4]Institute of Materials Research, Helmholtz-Zentrum Geesthacht, Max-Planck-Str. 1, 21502 Geesthacht, Germany

Abstract

The Interdependence model will be briefly reviewed and then applied to two different casting situations. One is the solidification of Mg-Al-Sm alloys to determine the optimum composition for achieving a fine as-cast grain size. Because the size range of the nucleant particles can be measured, the key factors describing the potency of the particle can be calculated providing a more complete description of the grain formation mechanisms operating for this alloy. This approach should be relevant for other Mg-Al-RE alloys. The other casting situation is where the melt of an AM60 - AlN nanoparticle composite was treated ultrasonically producing a fine grain size on solidification. The limitations to grain size reduction by nanoparticles are discussed in terms of the Interdependence and Free Growth models.

Key Words: Interdependence model; nucleation; magnesium alloys; solidification; ultrasonic treatment.

1. Introduction and the Interdependence Model

To obtain optimum mechanical performance a uniform fine equiaxed grain size is usually required. Equiaxed solidification and refinement of the as-cast grain size can be accomplished by: the addition of solute elements with a high value of the growth restriction factor Q*; inoculation by potent nucleant particles with low nucleation undercooling ΔT_n (i.e. high nucleation potency); a fine distribution of these particles within the melt; and controlling solidification parameters. (* $Q = mC_0(k-1)$ where m is the slope of the liquidus temperature in a binary phase diagram at a given alloy composition C_0, and k is the partition coefficient of the solute element between the solid and liquid phases.)

An example where the above factors play a role is provided by the application of UltraSonic Treatment (UST) of a range of Mg – Al alloys [1]. The results of this study are presented in Fig. 1 where grain size decreases as the value of Q increases and the intensity of UST is increased. In this example, it is not known precisely which compounds act as the nucleants but Fig. 1 shows that as the UST intensity increases the number of nucleant particles that can be activated (related to the y-axis intercept) also increase. Fig. 1 highlights the significant effect of alloy composition, nucleant particles and casting environment on the grain size achieved. The grain size data allows a linear relationship between grain size and $1/Q$ to be plotted and this simple linear form assists the determination of the mechanisms affecting the final as-cast grain size. The slope of the $1/Q$ plots indicates the potency of the nucleant particles where a lower slope means a more potent particle. To conclude that a change in slope means a change in potency assumes that the casting conditions remain constant because other factors such as the temperature gradient can also change the slope. In order to understand why these factors affect grain size we need to understand the role of constitutional supercooling (CS).

As a grain grows, solute is rejected and builds up in the liquid at the solid-liquid interface generating a concentration gradient in front of the interface as shown in Fig. 2(a). In Fig. 2(b), this concentration gradient is converted to a gradient of the equilibrium temperature T_E. The CS zone exists where the actual temperature gradient of T_A is lower than the equilibrium temperature T_E. The temperature difference between T_E and T_A is ΔT_{CS}. The size of the ΔT_{CS} zone and the peak value of ΔT_{CS} govern the extent of equiaxed grain nucleation [2]. When the gradient of T_A is relatively steep as shown schematically in Fig. 2(b), the casting conditions favour directional solidification of columnar grains. In contrast, Fig. 2(c) represents the ideal situation for the production of a fully equiaxed structure. Also required are potent nucleant particles to trigger the nucleation of grains. The important properties of the nucleant particles, whether naturally present in the alloy melt or deliberately added as inoculants, are their nucleation potency, defined by ΔT_n, and their distribution and number density, which define the spacing x_{Sd} between nucleated grains.

Fig. 2 highlights a challenge to overcome which was revealed during the development of the Interdependence Theory [3]. This is the formation of a Nucleation-Free Zone (NFZ) around each successfully nucleated grain where nucleation is unlikely to occur. The length of NFZ, x_{nfz}, includes the length of the diffusion field as marked on the schematic of Fig. 2(c) plus the amount of growth of the grain needed to generate sufficient ΔT_{CS}. The size of x_{nfz} depends on a number of factors as shown by the Interdependence equation, Eq. 1.

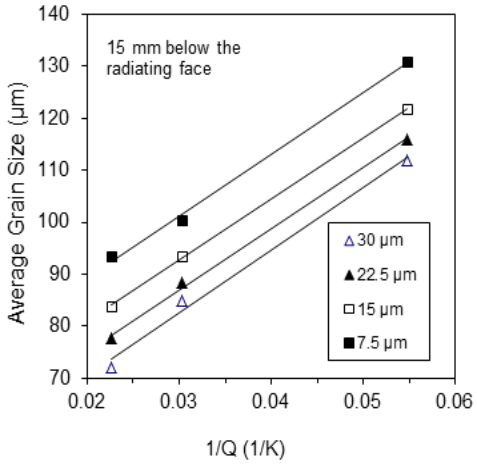

Figure 1. Grain size versus Mg-Al alloy Q values, subjected to UT amplitudes between 7 and 30μm**.** [1].

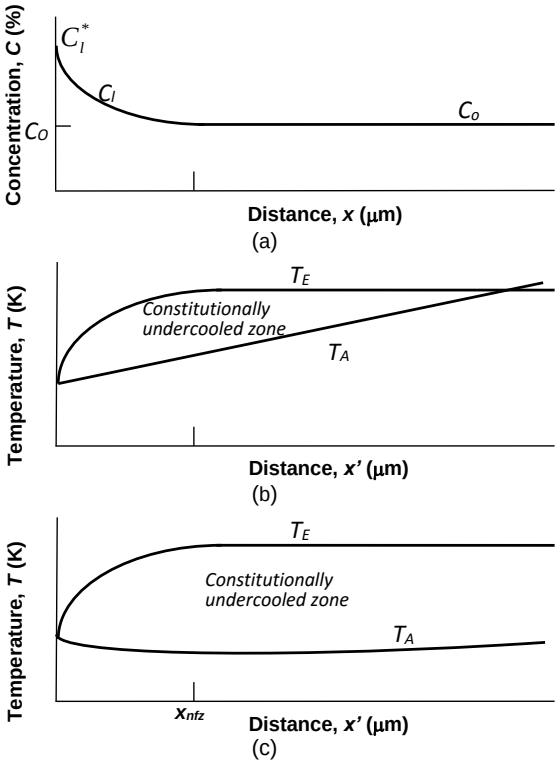

Figure 2. Schematics of (a) the solute concentration in front of a growing solid-liquid interface; (b) the concentration gradient converted to the equilibrium liquidus temperature T_E where the constitutionally supercooled zone is the difference between T_E and the actual temperature T_A and the gradient of T_A, G, is typical of directionally solidified alloy; and (c) represents the case of equiaxed solidification in a low temperature gradient. x_{nfz} denotes the end of NFZ. (from [4]).

The Interdependence equation (Eq. 1) [3] shows the relationship between constitutional supercooling and particle characteristics in defining the distance between nucleation events and, therefore, is a predictor of the relative grain size, d_{gs}.

$$d_{gs} = \frac{D \cdot z\Delta T_{n-min}}{vQ} + \frac{4.6D}{v} \cdot \left(\frac{C_l^* - C_0}{C_l^* \cdot (1-k)} \right) + x_{Sd} \qquad (1)$$

where D is the solute diffusion coefficient, $z\Delta T_{n\text{-}min}$ is the incremental amount of undercooling needed to trigger nucleation on the most potent particle of potency $\Delta T_{n\text{-}min}$, v the growth velocity of the interface, C_o the alloy composition, C_l^* the liquid composition at the interface, and k the partition coefficient. The term z is related to the temperature gradient of T_A.

The three terms of Eq. 1 define the distance between nucleation events where

$$d_{gs} = x_{CS} + x'_{dl} + x_{Sd} \quad (2)$$

x_{CS} is the amount of growth of a previous grain to generate $\Delta T_{CS} = \Delta T_n$,
x'_{dl} is the length of the diffusion field to where ΔT_n is achieved, and
x_{Sd} is the average distance to the next most potent particle that successfully nucleates a grain.

Fig. 3 illustrates the relationship between these distances and shows the effect of alloy composition as represented by Q, on the grain size. Therefore, a key strategy for generating a fine equiaxed grain size is to reduce both the size of the nucleation free zone x_{nfz} and the spacing between the most potent particles x_{Sd}.

Fig. 4 illustrates the effect of the particle potency ΔT_n on x_{nfz} and on the achievable grain size. As the nucleation temperature decreases (i.e. ΔT_n increases) the size of x_{nfz} increases as more growth is needed for ΔT_{CS} to equal or exceed ΔT_n.

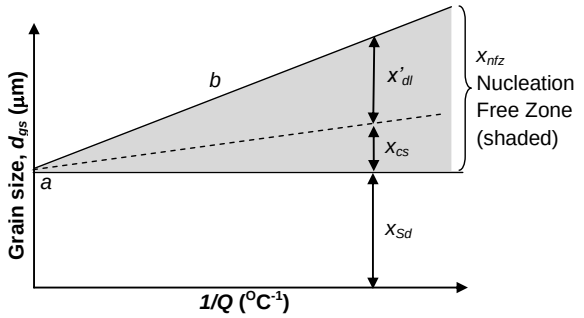

Figure 3. A representation showing the relationship between composition as defined by Q and the components in Eq. 2 that contribute to the grain size. x_{Sd} is constant if the number density of nucleant particles does not change with composition as shown in this figure (from [3]).

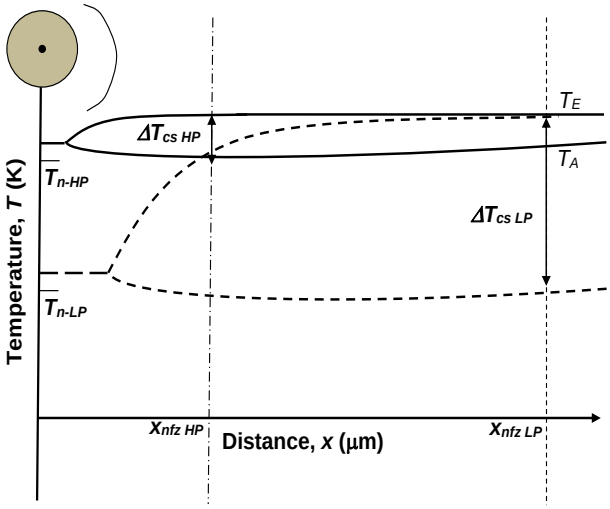

Figure 4. Schematic of the formation of the CS zone where a small $\Delta T_{CS\text{-}HP}$ forms for nucleant particles of high potency $T_{n\text{-}HP}$ and $\Delta T_{CS\text{-}LP}$ for low potency $T_{n\text{-}LP}$ particles. The high potency particles lead to a much smaller NFZ of $x_{nfz\text{-}HP}$ than the low potency particles at $x_{nfz\text{-}LP}$.

The Interdependence model is so named because the grain size is dictated by the interaction between CS and the particle characteristics ΔT_n and x_{Sd} in Eq. 1. Since there is a range of particle sizes as shown by the example presented in Fig. 5(a), the average distance between particles will differ for particles of different values of ΔT_n. According to the Free Growth model ΔT_n is related to the size of the particles by the following equation

$$\Delta T_n = 4\sigma/(\Delta S_v.d) \quad (3)$$

where σ is the solid-liquid interfacial energy and ΔS_v the entropy of fusion. S_d is calculated for each value of ΔT_n from the distribution in Fig. 5(a) where $S_d = 100\mu m/N_d$ and N_d is the number of particles within 100µm. Bringing these calculations together generates Fig. 5(b). The addition of further master alloys shifts the curves to the left reducing S_d and therefore the grain size. This approach was applied to the addition of Zr refiner to magnesium to compare the refinement efficiency of three Zr master alloys [5].

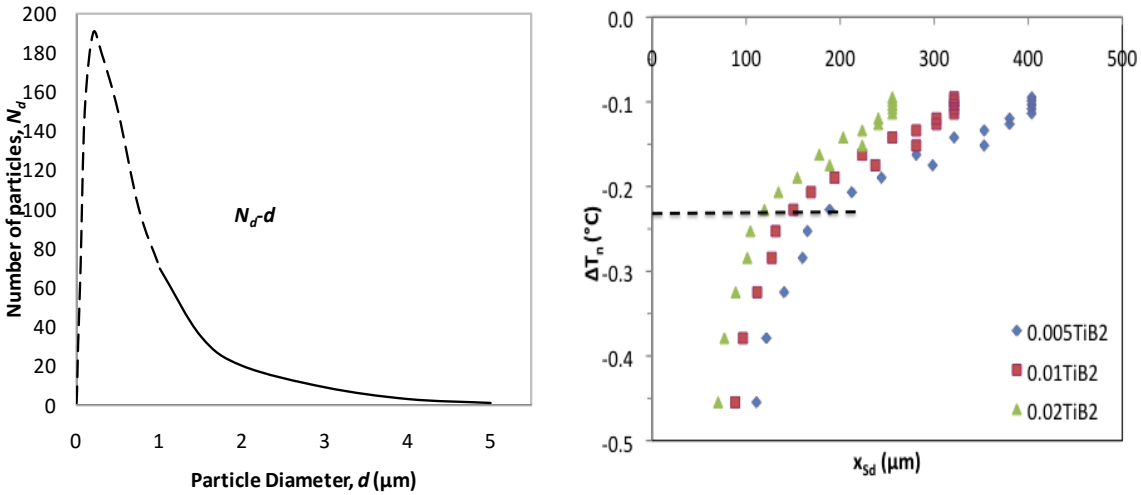

Figure 5. (a) The size distribution of particles based on TiB_2 size data from an Al5Ti1B master alloy [6]. (b) Using Eq. 3, the particle size and its distribution in (a) are transformed to a plot of nucleation undercooling ΔT_n versus the average distance between particles x_{Sd} of that value of ΔT_n.

Fig. 6 brings together the development of CS and the ΔT_n-S_d curve highlighting that nucleation occurs at the intersection of the gradient of T_A and the ΔT_n-S_d curve at time t_2.

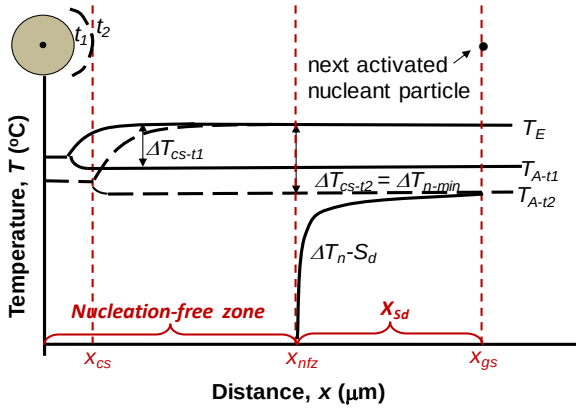

Figure 6. Schematic showing the relationship between the development of ΔT_{CS} from time t_1 to t_2 and the ΔT_n-S_d curve of the distribution of particles over a range of ΔT_n values. When the ΔT_n-S_d curve intersects T_A-t_2 temperature gradient a nucleation event will occur.

A recent review [7] discussed the benefits and limits of constitutional supercooling's effect on grain nucleation. The main limitation is the formation of NFZ. However, this is balanced by the facilitation of the formation of an equiaxed zone of fine grain size by the generation of ΔT_{CS} and the protection of newly nucleated grains from remelting while these grains are subjected to convection and transport throughout the melt during casting. The following two examples show how application of the Interdependence model provides an explanation of the mechanisms occurring during solidification that lead to the refinement of equiaxed grains. These examples were chosen because the mechanisms that make the largest contribution to the as-cast grain size are different. In the first example the number of nucleant particles plays an important role and in the second example the alloy chemistry and potency of the particles have a significant impact on the as-cast grain size.

2. Grain size variation of an Mg-Al-Sm alloy

In a recent publications [8,9] it was shown (Fig. 7) that a ternary addition of Sm (Samarium) to the Mg-3Al alloy firstly coarsened the grain size and then refined the grain size as the Sm composition was increased from 0 to 2.1 wt.%. A thermodynamic analysis [10] of the Mg-Al-Sm system calculated that the pro-eutectic Al_2Sm phase begins to form above 1.3 wt.%Sm. This factor plus observation of Al_2Sm particles in the center of grains in both 1.4 and 2.1 wt.% Sm samples and a crystallographic misfit of 0.45% with magnesium [8] clearly indicates that Al_2Sm is a good nucleant for magnesium. (The cause of coarsening from 0 to 0.7 wt.% Sm was found to be due to the transformation of the native Al-Fe-C-O particles to lower potency Al-Fe-Sm-C-O particles [8].)

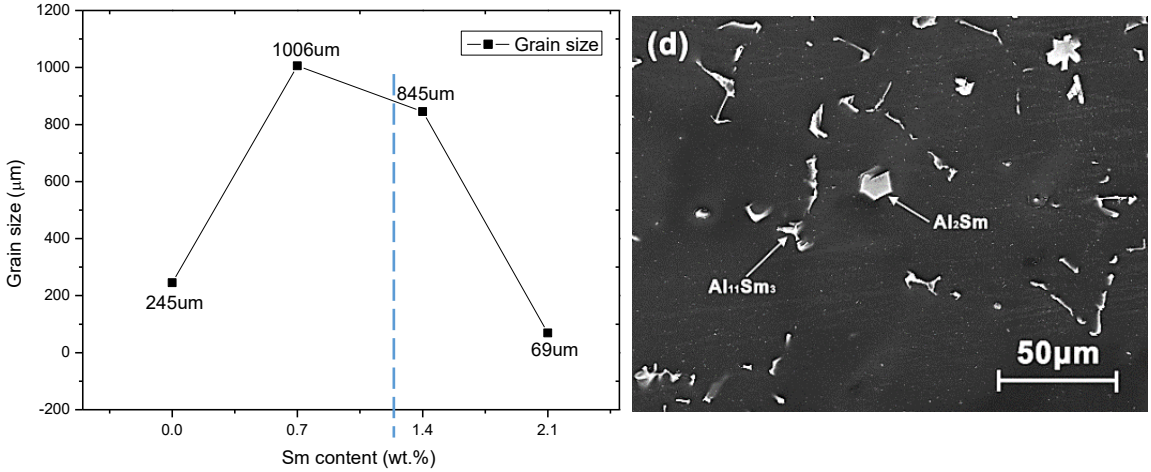

Figure 7. (a) Grain size versus Sm content, (b) SEM image of the Mg-3Al-2.1Sm alloy [8].

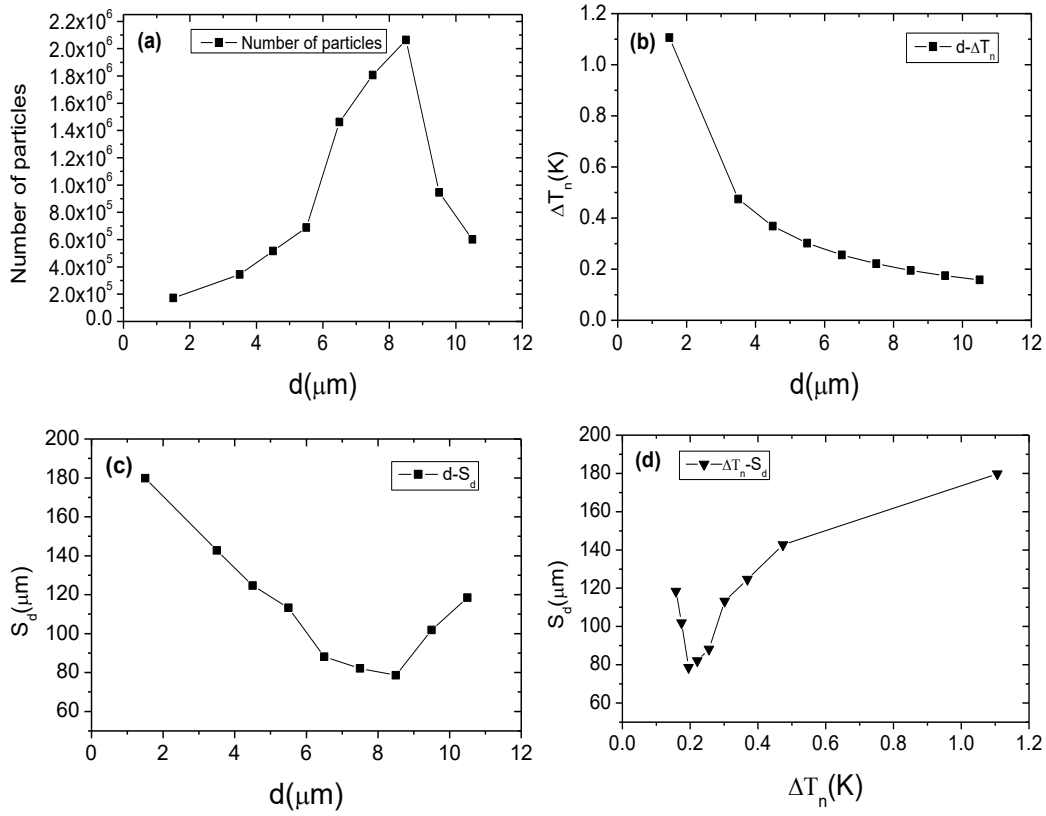

Figure 8. Characteristics of the Al_2Sm particles in the Mg-3Al-2.1Sm alloy. (a) the distribution N_d of the number of potent particles for each value of diameter *d*. (b) The relationship between nucleation undercooling ΔT_n and *d*. (c) Relationship between the average particle spacing *Sd* and particle size *d*. (d) S_d versus ΔT_n. [8]

Because the Al_2Sm particles are clearly visible in the microstructure (Fig. 7(b)), the size and their number were readily measured (Fig. 8(a)). Fig. 8(b) converts the sizes in 8(a) into values of ΔT_n by Eq. 2. Fig. 8(c) converts the number distribution in 8(a) to an average distance S_d versus particle size and Fig. 8(d) generates a plot of S_d versus ΔT_n which is used in Fig. 9.

Fig. 9 was constructed based on the schematic in Fig. 6 and the data in Fig. 8(d). This was the first time that there has been sufficient data to make a quantitative figure of the representation in Fig.6. Fig. 8(d) indicates the value of ΔT_n is less than 0.2 K which is reasonable as the crystallographic misfit is very low. The low value of ΔT_n plus the small value of z due to a relatively low temperature gradient in the melt means that x_{nfz} will be small. Thus, the grain size above 1.3 wt.%Sm is controlled by the size of x_{Sd}. Regarding x_{Sd}, the average spacing between the largest most potent particles is 120 μm. However, the as-cast grain size is 69 μm. To achieve this value all of the particles with a potency above 0.2 K must be activated which gives an x_{Sd} of 60 μm. Therefore, x_{nfz} must be small at about 10 μm as indicated above. Thus, in this example the major contributor to grain size is the number of particles able to successfully nucleate a grain.

From Fig. 9, Eq. 1 can be simplified to be a predictive equation for compositions above 1.3 wt.% Sm to $d_{gs} = 10\ (x_{nfz}) + (1000 - 1175 \times (C_o - 1.3))\ (x_{Sd}$ *where 1.3 <Co < 2.2 wt.%Sm*).

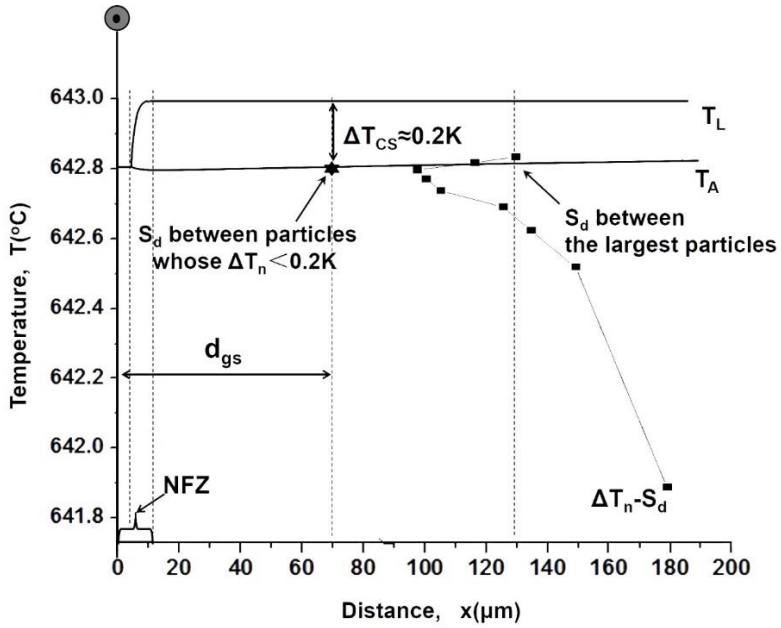

Figure 9. A schematic that illustrates the interrelationship between the development of ΔT_{CS} between the equilibrium liquidus temperature T_E and the actual temperature of the melt T_A, and the distribution of particles for the range of particle sizes converted to their nucleation undercooling (ΔT_n-S_d) that together establish the grain size of the Mg-3Al-2.1Sm alloy [8].

3. UST assisted grain refinement of an AM60 alloy containing AlN nanoparticles

Ultrasonic treatment can refine the grain size by treating the molten alloy or by application during the nucleation stage of solidification or by combining both methods [11]. In this example the former approach is taken where UST is applied above the liquidus temperature to ensure well-wetted nanoparticles and their uniform distribution throughout the melt [12]. One weight percent of AlN powder was added to the AM60 melt, stirred, UST applied for 5 minutes, and then the melt was poured into a 100 mm diameter cylinder which was lowered into a water bath for directional solidification from the bottom of the cylinder. In one gram of AlN powder there are about $1.15*10^{15}$ particles with an average size of 80 nm (Figure 10). The largest particles are 162 nm in size and represent 0.003 % of the total number of particles.

Figure 12 shows the effect of nanoparticles on grain size where UST of AM60 has a grain size of 1277 μm while UST of AM60 with AlN particles has a grain size of 85 μm. By converting the number of particles per gram to the number of particles per volume of the nanocomposite, the average spacing between the largest particles is 2.1 μm. Thus, the grain size would be 2.1 μm if we assume all of the largest particles are the most potent and nucleate a grain. However, the measured grain size is 85 μm. This means that only a very small fraction (approximately 0.002 %) of the largest 0.003 % of particles successfully nucleate a grain.

Considering Eq. 1, the very high number density of nucleant particles implies x_{Sd} would be small, probably < 5 microns. Thus, changes in grain size would be largely affected by changes to the size of the nucleation-free zone which was also found to be the case for Mg-Al alloys without particle additions [3]. A key factor in determining the size of NFZ is the nucleation undercooling of the particles. ΔT_n was measured by DSC to be 14 K. The high value of ΔT_n would be expected according Eq. 2 for very small particle sizes. Based on calculations of x_{nfz} used previously [3] x_{nfz} is predicted to be ~ 600 μm which is much larger than 85 μm. The main parameters in Eq. 1 that could reduce the size of x_{nfz} are D and v as Q has not changed. V may be faster due to the casting rate of 3 mm/s. It is also possible that high levels of nanoparticles reduce the effective diffusion coefficient. An indication of a decrease in D can be caused by a decrease in viscosity [13]. This is supported by spiral fluidity measurements where the spiral length decreased by about 14% from 96.2 to 83.5 cm when AlN particles are added. In order to decrease x_{nfz} to less than 90 μm D needs to be reduced from $5x10^{-9}$ to $7x10^{-10}$ m^2/sec. This hypothesis regarding a relationship between viscosity and diffusion coefficient needs verification by further research.

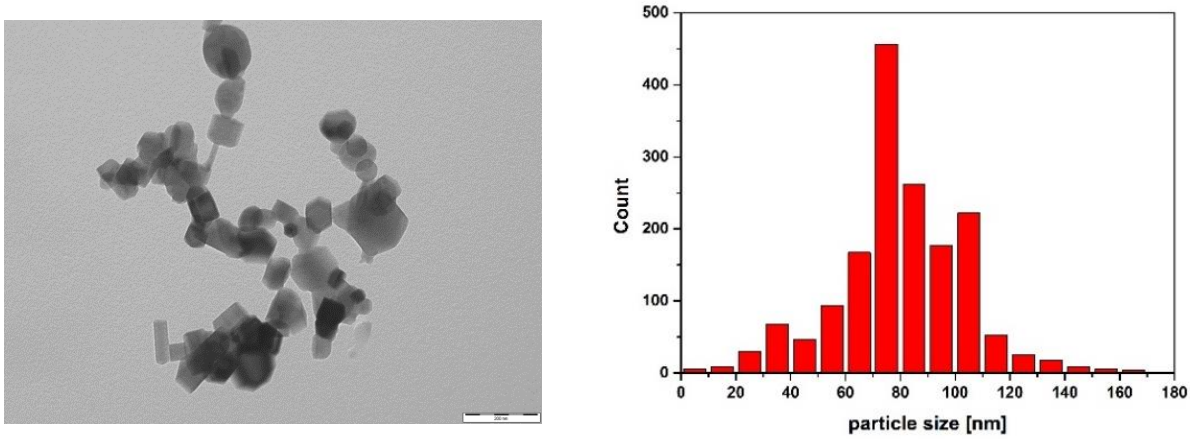

(a) (b)

Figure 10. (a) Typical AlN nanoparticles and (b) particle size distribution of the AlN nanoparticles [12].

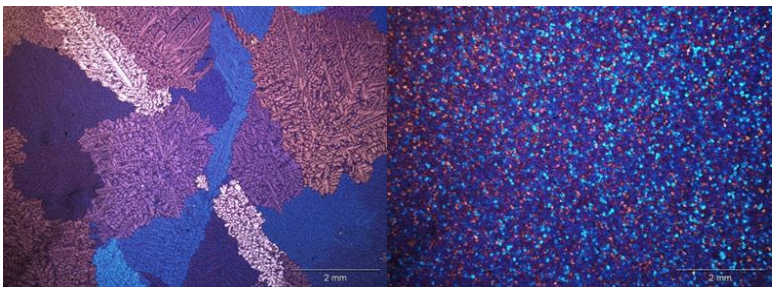

(a) (b)

Figure 11. Microstructure and grain size of (a) AM60, 1277 ± 300 μm and b) AM60+AlN, 85 ± 6.2 μm [12].

Understanding the formation of NFZ is critical to improving the performance of nanoparticles as nucleants because the dominant effect of NFZ will impact on the mechanical properties through the Hall-Petch relationship. In a broader study of the AM60-AlN system, a Hall-Petch relationship with grain size was found despite the very large number density of nanoparticles [12].

4. Concluding remarks

The two examples described above show that the Interdependence model is a framework for determining whether x_{nfz} or x_{Sd} make a greater contribution to grain size, and therefore provides a focus for identifying methods to decrease the grain size. In the Mg-Al-Sm example x_{Sd} has the predominant effect on grain size while for the AM60-AlN nanocomposite example the size of x_{nfz} controls the grain size. In the case of the nanocomposite the very small particle size results in a large NFZ preventing very small grain sizes being formed. This effect may be applicable to other nanocomposite alloy systems.

The Interdependence model can be used to:

- understand the sometimes complex interaction between factors affecting nucleation and grain refinement;
- highlight the importance of NFZ;
- understand why NFZ prevents the formation of very fine grain sizes in AlN nanocomposites (assuming particle pushing does not occur); and
- analyse the effect of a range of solidification conditions on grain size.

Acknowledgements

DStJ acknowledges the support of Australian Research Council grants DP 140100702 and DP160100560. XH acknowledges the support of the National Natural Science Foundation of China (No. 51201103), SJTU Special Funds for Science and Technology Innovation (No. 13X100030018), and the Program for Outstanding Academic Leader of Shanghai (14XD1425000). The authors thank Penghuai Fu, Mingxing Zhang, Lydia Katsarou, Ricardo Buzolin, Gabor Szakacz, Manfred Horstmann, Martin Wolff, Chamini Mendis and Sergey Vorozhtsov for their contribution to the research on the two examples. Stuart McDonald and Arvind Prasad are thanked for calculating the composition of the Al_2Sm phase boundary and providing advice on the relationship between viscosity and the diffusion coefficient, respectively. HD and DStJ wish to acknowledge financial support from the European Commission (ExoMet Project, 7th Framework Programme, contract FP7-NMP3-LA-2012-280421).

References

1. A. Ramirez A, Das A, StJohn DH (2010) The effect of solute on ultrasonic grain refinement of magnesium alloys. Journal of Crystal Growth 312: 2267-2272

2. Prasad A, Yuan L, Lee P, Easton M, StJohn D (2016) The effect of the melt thermal gradient on the size of the constitutionally supercooled zone, in: IOP Conference Series: Materials Science and Engineering, IOP Publishing, 012001

3. StJohn DH, Qian M, Easton MA, Cao P (2011) The Interdependence Theory: the relationship between grain formation and nucleant selection. Acta Mater, 59:4907-4921

4. Polmear I, StJohn D, Nie JF, Qian M (2017) Light Alloys: Metallurgy of the Light Metals, 5th ed., Butterworth-Heinemann

5. Sun M, Easton MA, StJohn DH, Wu G, Abbott TB, Ding W (2013) Grain Refinement of Magnesium Alloys by Mg-Zr Master Alloys: the Role of Alloy Chemistry and Zr Particle Number Density, Advanced Engineering Materials 15(5): 373-378

6. Greer AL, Bunn AM, Tronche A, Evans PV, Bristow DJ (2000) Modelling of inoculation of metallic melts: application to grain refinement of aluminium by Al–Ti–B. Acta Mater. 48:2823-2835

7. StJohn DH, Prasad A, Easton MA, Qian M (2015) The contribution of constitutional supercooling to nucleation and grain formation. Metall. Mater. Trans. A 46:4868–4885

8. Hu X, Fu P, StJohn D, Peng L, Sun M, Zhang M (2016) On grain coarsening and refining of the Mg-3Al alloy by Sm. Journal of Alloys and Compounds 663: 387-394

9. Ming Sun, XiaoyuHu, LimingPengn, PenghuaiFu, YinghongPeng (2014) Effects of Sm on the grain refinement, microstructures and mechanical properties of AZ31 magnesium alloy. Mater. Sci. &Eng. A 620:89–96

10. Jin L, Kevorkov D, Medraj M, Chartrand P (2013) Al–Mg–RE (RE = La, Ce, Pr, Nd, Sm) systems: Thermodynamic evaluations and optimizations coupled with key experiments and Miedema's model estimations. J. Chem. Thermodynamics 58: 166–195

11. Wang G, Dargusch MS, Eskin DG, StJohn DH (2017) Identifying the Stages during Ultrasonic Processing that Reduce the Grain Size of Aluminum with Added Al3Ti1B Master Alloy. Advanced Engineering Materials DOI: 10.1002/adem.201700264

12. Dieringa H, Katsarou L, Buzolin R, Szakacz G, Horstmann M, Wolff M, Mendis C, Vorozhtsov S, StJohn D (2017) Ultrasound assisted casting of an AM60 based metal matrix nanocomposite, its properties and recyclability. Submitted for publication August 2017

13. D.R. Poirier (2014) Density, viscosity, and diffusion coefficients in hypoeutectic Al-Si liquid alloys: an assessment of available data. Met. Mater. Trans. B 45B:1345-1354